Effect of Nanoscopic Fillers on Dewetting Dynamics

**J. H. Xavier,*,[†] S. Sharma,[†] Y. S. Seo,[†] R. Isseroff,[§] T. Koga,[†] H. White,[†] A. Ulman,[‡]
K. Shin,[⊥] S. K. Satija,[#] J. Sokolov,[†] and M. H. Rafailovich*,[†]**

*Department of Materials Science and Engineering, State University of New York at Stony Brook,
Stony Brook, New York 11794; Department of Chemical Engineering and Chemistry, Polytechnic
University, Brooklyn, New York 11201; Stella K. Abraham High School, Hewlett, New York 11557;
Department of Science and Engineering, Gwanju Institute of Science and Technology,
Gwanju, 500-712, Korea; and Center for Neutron Research, National Institute of Standards and
Technology, Gaithersburg, Maryland 20899*

ABSTRACT: We synthesized C_{18}-functionalized gold and palladium nanoparticles with average diameter size of 10 and 3 nm, respectively, and carried out a systematic study of the effect of nanoscale metallic fillers on the dewetting dynamics of PS/PMMA bilayer substrates. Optical and atomic force microscopies were used to study the hole growth and determine the viscosity of the films as a function of PS molecular weight, particle radius, and concentration. Neutron reflectivity was used to measure the effects of the nanoparticles on the tracer diffusion coefficient. X-ray reflectivity and TEM microscopy were used to study the distribution of the particles within the film and ensure that no segregation or clustering occurred. The results indicated that the dynamics are a sensitive function of the ratio between the filler radius, $R_{particle}$, and the polymer radius of gyration, R_g. The data were found to collapse on a universal curve where the relative velocity of the filled system was faster than that for the unfilled system when $R_g/R_{particle} > 4$ and slower when $R_g/R_{particle} < 4$. Shear modulation force microscopy method (SMFM) measurements were performed as a function of temperature and indicated that T_g was depressed by 12 °C relative to the bulk when $R_g/R_{panrticle} > 4$ and unchanged when $R_g/R_{particle} < 4$. The results were interpreted in terms of an increase in the local excluded volume and possible elastic distortions of the polymer matrix.

Introduction

Nanoscale noble metal and metal oxide particles have been added to polymers for years to significantly enhance various properties such as UV absorption, electrical conductivity, and optical dispersion.[1−3] In contrast to bulk fillers, such as carbon black or silica, which are added in large quantities in order to reinforce structural properties,[4] the concentration of metallic particles required to affect the electronic response is often less than 5%. Therefore, it has always been assumed that these metal fillers have no effect on the rheological or mechanical properties. Furthermore, since these nanoparticles are coated with surfactants used as dispersants, it has been assumed that they do not interact with the polymer chains and hence do not affect properties such as viscosity, glass transition, or interfacial tensions. Thus, not much attention has been given to the effect of fillers on film stability, which is governed only by known differences in the surface and interfacial energy of the polymers.

Recently, several authors have shown that dewetting can be greatly affected when strong interactions exist between the fillers and the substrate or the polymer matrix. Barnes et al.[5] have shown that the addition of C_{60} can stabilize homopolymer films against dewetting. In this case, segregation of the C_{60} filler to the substrate created a surface, which interacted strongly with the polymer and suppressed dewetting by pinning the polymer chains. This situation was also modeled by Gersappe et al.[6]

Sharma et al.[7] have shown that when the filler interacts strongly with the polymer matrix, dewetting can be either accelerated or arrested depending on the sign of the interaction. In most applications, though, segregation of fillers is not desirable, and surfactants[8] are used to keep the fillers well dispersed within the matrix. In the current investigation, we focus on the study of the rheological properties of films with functionalized metallic nanoparticle fillers, where only weak van der Waals interactions exist between either the particles and the polymers or the substrate. The effects on viscosity were first addressed by Cole et al.[9] and found an increase in viscosity when attractive interactions existed between evaporated Au particles and the matrix. Mackay et al.[9] reported a similar effect using cross-linked polymer particles.

We use a technique developed by Qu et al.[10] where we observe the rate of dewetting in polymer bilayer films and apply the theory of Brochard-Wyart et al.[11] to extract the viscosity of the films. We show that even in the case where particles are well dispersed in the films, large effects on the stability of the film due to dewetting may be induced by the addition of fillers.

We compare the case for two types of nanoparticles, Au and Pd, formed by the one-phase synthesis method described by Ulman and co-workers[12] and functionalized with the same octadecanethiol ($C_{18}H_{37}SH$) molecules. Optical and lateral force microscopies are used to study the growth rate of holes and position of the particles during the dewetting process as a function of time and particle concentrations. Results were complemented by specular X-ray reflectivity and transmission electron microscopy (TEM), which profiled the distribution of the particles. Neutron reflectivity was also used to study the effects of the particles on the tracer diffusion coefficient of the polymers. We show that even though all interactions in the system are the same, the particle size relative to the radius of gyration of the polymer chain seems to be the predominant factor affecting film stability.

[†] State University of New York at Stony Brook.
[‡] Polytechnic University.
[§] Stella K. Abraham High School.
[⊥] Gwanju Institute of Science and Technology.
[#] National Institute of Standards and Technology.
* Corresponding authors: Tel 631-632-8483, Fax 631-632-5764, e-mail jeanharry.xavier@gmail.com, mrafailovich@notes.cc.sunysb.edu.
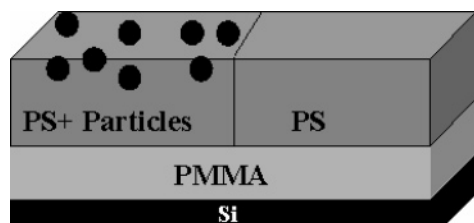
Figure 1. Geometry of a PS/PMMA bilayer film on a Si wafer. The PMMA film is adjacent to the substrate. The upper PS layer contains two parts; one-half is filled with particles, and the other is unfilled.

Table 1. Characteristics of Polymers Used in This Study

polymer	mol wt (g/mol)	thickness (Å)	polydispersity	melt viscosity[28] (162 °C) (Pa s)
PS	65K	240	1.6	11×10^3
PS	90K	240	1.7	34×10^3
PS	123K	240	1.3	1×10^5
PS	650K	260	1.8	3×10^7
PS	1.0M	280	1.1	1×10^8
PS	4.0M	280	1.4	1×10^{10}
PMMA	330K	280	1.1	2.4×10^8
PMMA	650K	280	1.4	$\sim 10^{10}$

Theoretical Background. Consider a bilayer film composed of the immiscible polymers, PS/PMMA, as shown in Figure 1. The sample is constructed such that half of the PS layer contains particles and the other half is unfilled. The dewetting is controlled by the spreading parameter, S, which quantifies the balance between minimizing interfacial area and presenting the polymer with the lowest surface tension at the vacuum interface.

$$S = \gamma_B - (\gamma_A + \gamma_{AB}) \tag{1}$$

Here γ_B, γ_A, and γ_{AB} are the surface tensions of the bottom, top layers, and the interfacial tension between the two layers, respectively.

In thin films, dewetting can be initiated by capillary instabilities,[13,14] which result in spontaneous formation of holes in the upper layer. These instabilities may arise from the difference in the amplitude of the capillary waves at the free surface and the polymer interface. If $S < 0$, the total energy of the system is lowered by exposing the substrate, and the holes grow with a dewetting velocity, V. In the case where the viscosity of the upper layer, η_A, is lower than that of the upper layer, Brochard-Wyart et al.[11] have shown that V is constant and independent of the viscosity of the lower layer, η_B. In this case, known as the "solidlike lower layer regime", the viscosity is given by

$$V \propto [12 \times 2^{1/2}]^{-1} (\gamma_A / \eta_A) \theta_e^3 \tag{2}$$

where $\cos \theta_e = (\gamma_B - \gamma_{AB})/\gamma_A$. Hence, if the parameters in eq 2 are known for a given set of polymers, Qu[10] has shown that one can use eq 2 to determine the viscosity of the film. Here we use this technique to compare the effect of adding fillers into the homopolymer film's viscosity.

We will use bilayers of the immiscible blend, poly(methyl methacrylate) (PMMA) and polystyrene (PS), where we varied the molecular weight of the PS upper layer such that $\eta_{PMMA} > \eta_{PS}$. Hence, in this geometry V is inversely proportional to η_{PS}, and we probe only the viscosity of upper layer where the nanoparticles will be introduced. We will then be able to compare, under identical thermal conditions and substrate interactions, the effect of fillers on the viscosity of thin PS films. The viscosity of each layer is listed[10] in Table 1.

Experimental Section

One-Phase Synthesis of Thiol-Functionalized Nanoparticles. The gold and palladium nanoparticles were prepared using the one-phase synthesis method developed by Ulman and co-workers.[12] The synthesis procedure involved the addition of 0.47 mg of octadecanethiol ($C_{18}H_{37}SH$, ODT), under vigorous stirring, to a solution of 0.7 mmol of hydrogen tetrachloroaureate (111) trihydrate ($H[Au-(Cl_4)]\cdot 3H_2O$) or ($[Pd(C_2H_3O_2)_2]_3$) in 10 mL of THF for the Au and Pd particles, respectively. The mixture was stirred for ~20 min at room temperature. A solution of lithium triethylborohydride was added dropwise until the mixture turned a dark red-brown color. The resulting solution was centrifuged four times at 8000 rpm in methanol to remove unattached organics. The methanol was decanted, and then the residue was dried in a vacuum for 4−6 h.

Sample Preparation Technique. Polystyrene (PS) and poly-(methyl methacrylate) (PMMA) of various molecular weights were used in this study. PMMA was chosen as the lower layer since the interfacial energy of silicon with PMMA is smaller than that with PS. (The silicon wafers used in the experiment were first cleaned by sonicating in toluene to remove organic residues.) The surfaces were then cleaned using a modified Shirake technique,[15,16] which was previously shown to produce a uniform native oxide layer (~20 Å). This procedure consists of immersion for 10 min in 25% H_2O_2 hydrogen peroxide solution, stripping with 15% HF water solution, and finally rinsing thoroughly with distilled water and drying under flowing nitrogen at room temperature.

Solutions of monodisperse PS and PMMA of the molecular weights listed in Table 1 were prepared in toluene. C_{18}-functionalized Pd and Au (weight percentages ranging from 1% to 4%) nanoparticles were added to some of the PS solutions, which were further sonicated for 1 h. (It should be noted that the volume fraction ranges from 5×10^{-5} to 2×10^{-3} for the Au particles and from 8×10^{-5} to 3×10^{-3} for the Pd particles.) The solution appeared to be stable, indicating the particles are miscible with the polymer.

A schematic of the sample geometry is shown in Figure 1. A film of PMMA ($M_w = 306K$) was first spun-cast directly onto the cleaned Si wafer. The thickness of the film was measured with ellipsometry, 28 nm. The error in measuring the film thickness with ellisometry is less than 1%. The PS solution with particles was then spun-cast onto a glass slide and carefully floated from distilled water onto half of the PMMA substrate. Using the same process, a layer of PS without nanoparticles was floated onto the other half of the PMMA substrate. This procedure was done in order to allow for a direct comparison of the dewetting velocities of PS with and without particles under identical annealing conditions.

The samples were then inserted into a high-vacuum oven with a specially designed load lock chamber, which allowed for accurate temperature control even for short annealing times. The annealing temperature was fixed at 162 °C for Au and 168 °C for Pd. It should be noted that no dewetting of the PMMA underlayer at 160 °C was observed. The system vacuum during annealing was maintained at 10^{-7} Torr at all times. The heating element of the oven was wrapped around the entire exterior, and the heat propagated from the outside to the sample by convection. In this method, very uniform heating could be achieved. The spatial dependence of the thermal gradients in the oven was mapped using an infrared detector and found to be no larger than 1 deg over the dimensions of the sample. Hence, any differences due to temperature could be easily ruled out.

The glass transition, T_g, of the films was measured using the shear modulation force microscopy (SMFM) technique on a Dimension 3000 (Digital Instruments, Santa Barbara, CA). This method is described in refs 17 and 18 where we showed that it could accurately reproduce T_g in thin PS films on different substrates. The experiments were performed in a sealed glovebox, which was purged with dry nitrogen in order to maintain constant humidity. In this technique a sinusoidal drive signal was applied to the x-piezo to induce a small (3 nm) oscillatory motion at the tip, parallel to the sample surface. The amplitude of the response signal, Δx, was then fed through a lock-in amplifier and detected as a function of temperature. The amplitude response, Δx, is directly related to the zero frequency modulus and the tip sample contact area. At T_g, the modulus decreases by several orders of magnitude, causing a large and abrupt increase in discontinuity in Δx. Hence,
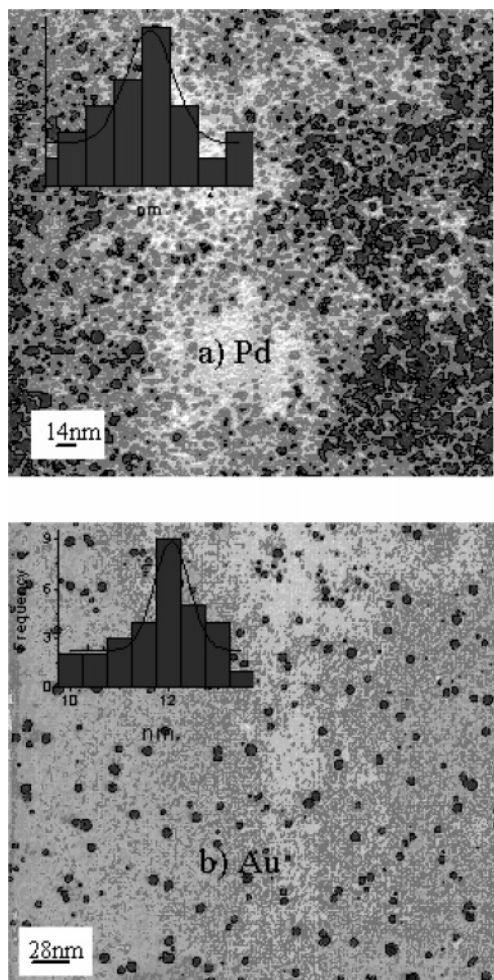
Figure 2. TEM micrographs showing the distribution in PS films (M_w = 123K) of (a) Pd nanoparticles and (b) Au nanoparticles. Histograms of the particle size [inset] show that the mean diameter for the Pd and Au particles are 3 ± 0.4 and 12 ± 0.7 nm, respectively.

as described in refs 17 and 18, by observing the temperature at which this occurs, we can determine the glass transition temperature, T_g, of the sample.

Particle Size Characterization. The particle size was determined by spin-casting onto a clean glass slide thin PS (M_w = 123K) films (~40 nm) with 1 wt % of either functionalized gold or palladium nanoparticles. The films were then floated from distilled water onto carbon-coated Cu grids and imaged with a Phillips CM-12 transmission electron microscope (TEM) at 100 keV. The results are shown in Figure 2, where we see that both Pd (a) and Au (b) particles were well dispersed within the PS matrix. The inset in each figure is a histogram of the particle size, where we see that the mean diameter for the Au and Pd particles are 10 ± 0.4 and 3 ± 0.7 nm, respectively.

Determination of the Interfacial Energy between PS and Thiol-Covered Au or Pd Surfaces. To determine the interfacial tension between thiol-covered Au or Pd particles surfaces and PS films, we allowed the films to completely dewet these surfaces and then observed the contact angles. The substrates were prepared by vapor evaporation of Au or Pd films, ~50 nm thick, onto Si wafers cleaned by the Shirake method.[15,16] The substrates were first cleaned by etching in the Ar$^+$ plasma and then placed in a 1 mM thiol [(C$_{18}$H$_{37}$SH) octadecanethiol] THF solution for ~1 min in order to produce a self-assembled thiol monolayer (SAM).

A PS (M_w = 123K) film ~28 nm thick was spun-cast onto the SAM and annealed at 165 °C for 4 days to achieve complete dewetting. The samples were then imaged with a DI-3000 atomic force microscope with a silicon nitrite tip in the contact mode using both topography and lateral forced mode. A cross-sectional analysis
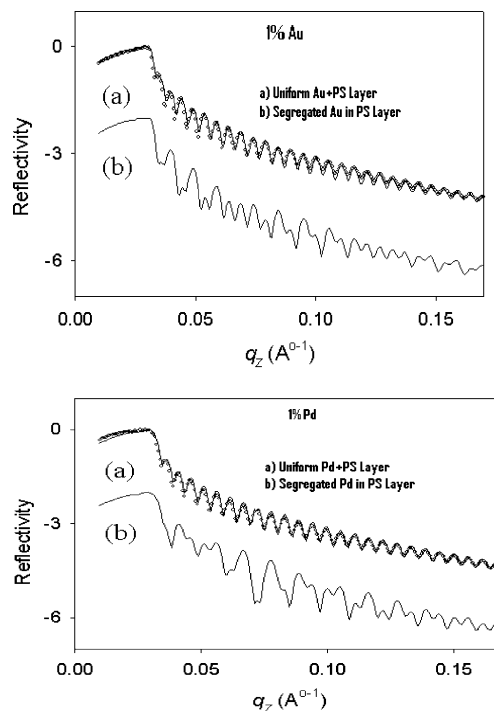

Figure 3. X-ray reflectivity of PS/PMMA bilayer films with nanoparticles, annealed for 1 h at 162 °C. The solid lines are the fits to data assuming a uniform particle distribution as shown in Figure 4 (solid line) below. The lower curves (particles segregated layer) are the calculated scattering intensity for the configurations shown in Figure 4 (dashed line). (a) PS layer containing 1% Au 10 nm diameter particles. (b) PS layer containing 1% Pd 3 nm diameter particles.

of the images yields a contact angle of θ = 12° and θ = 11° for the Au and Pd surfaces, respectively. The interfacial energy[19,20] between PS and the thiol-covered surfaces can be deduced from Young's relation.[21]

$$\gamma_{thiol} - \gamma_{PS/thiol} - \gamma_{PS} \cos \theta = 0 \qquad (3)$$

Substituting γ_{PS} = 30.26 dyn/cm and γ_{thiol} = 16.85 dyn/cm at 168 °C, we find that $\gamma_{PS/thiol}$ is = 7.1 dyn/cm for Au and 6.9 dyn/cm for Pd surfaces.[22] Hence, the interfacial tensions between and the two SAM-covered surfaces and the PS films are the same within experimental error.

X-ray and Neutron Reflectivity Measurements. The distribution of Au and Pd particles in the bilayer films following annealing was measured using X-ray reflectivity, while the diffusion coefficient was measured using neutron reflectivity.

X-ray Reflectivity. Bilayer films were made by spin-casting a 65.3 nm thick PMMA (M_w = 306K) film onto silicon substrates cleaned via the Shirake method.[15,16] A PS (M_w = 123K) film, 50.5 nm thick, containing 2% Au or 3 nm diameter Pd particles, was spun-cast onto a glass slide and floated on top of the PMMA substrate. The film thicknesses were chosen such that the annealing time, 1 h at T = 162 °C, would be sufficient to relax the polymer chains and yet be too short to initiate dewetting. Hence, only a small change in film thickness could effectively suppress dewetting and allow us to tailor the sample to the observation time. The measurements were performed at the Brookhaven National Laboratory (BNL), National Synchrotron Light Source (NSLS), beamline X10B, with an incident energy of 11 keV and wavelength λ = 1.13 Å.

The specular reflectivity data were measured as a function transverse momentum vector, $q_z = 2\pi \sin(q)/\lambda$, where θ is an incident angle. The reflected intensity of the data is plotted as a function of q_z for films with 10 nm diameter Au and 3 nm diameter Pd nanoparticles in parts a and b of Figure 3, respectively. From the figures we see that the data for both types of films have uniform oscillation with only a single frequency. The lines in the figures
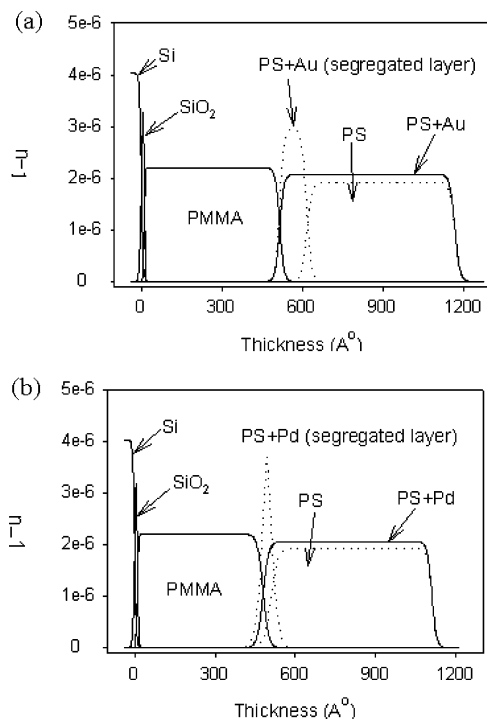
Figure 4. (a) Electron density profiles for PS films containing 1% Au particles corresponding to the solid lines used to fit the data in Figure 3a. Two models are tested; a uniform distribution (solid line) and a particle layer segregated to the PS/PMMA interface (dashed line). (b) Electron density profiles corresponding to the reflectivity data of PS films containing 1% Pd particles (Figure 3b). The solid line corresponds to the profile where the Pd particles are uniformly distributed in the PS layer (solid line), and the dashed line corresponds to the profile where the particles are segregated to the polymer/polymer interface.

correspond to the profiles plotted in Figure 4. The solid lines through the data in both figures correspond to the electron density profiles, where the nanoparticles are uniformly dispersed within the PS layer profiles below the data correspond to the profiles in Figure 4 where either the 10 nm diameter Au or 3 nm diameter Pd particles segregate to the PS/PMMA interface. This type of profile is easy to detect since the nanoparticles act as a separate layer with its own oscillation, providing the characteristic's beating pattern observed. Two models are proposed for fitting the data as shown in Figure 4. In the first model, the metallic particles remain uniformly distributed within the PS film. In this case the particles slightly increase the scattering length density of PS, such that it is matched to that of PMMA. This model is labeled either PS + Au or PS + Pd and is drawn as a dashed line in Figure 4. The fit to this model corresponds to the solid line profile superimposed upon the reflectivity spectra in Figure 4a,b, where it is seen to provide a good fit to the data. In the second model the particles segregate to the more polar PMMA interface, as shown by the dashed line profiles in Figure 4 and labeled PS + Au or PS + Pd, segregated in the figure. Because of the high scattering contrast between the polymer and the particles, even a concentration of 1% is sufficient to form a detectable adsorbed layer of particles. The reflectivity spectra that would result from the segregated profiles shown in Figure 3a,b are drawn as a dashed line in Figure 4. Here we clearly see that if a layer of particles had segregated to the interface, a distinct beating pattern between the Kiesig fringes of the polymer film and those from the higher contrast metal particle layer would have been observed. Hence, we conclude that the particles remain dispersed within the less polar PS matrix even after thermal annealing. Furthermore, we can rule out in this case the existence of a surface pinning layer such as the one postulated by Karim et al.[5] for C_{60} particles and calculated by Gersappe et al.[6] for the more general case of interacting particles (Figure 3a).

Neutron Reflectivity (NR). First, a layer of PS, $M_w = 200K$, 50 nm thick, was spun-cast from toluene solution onto the surface of
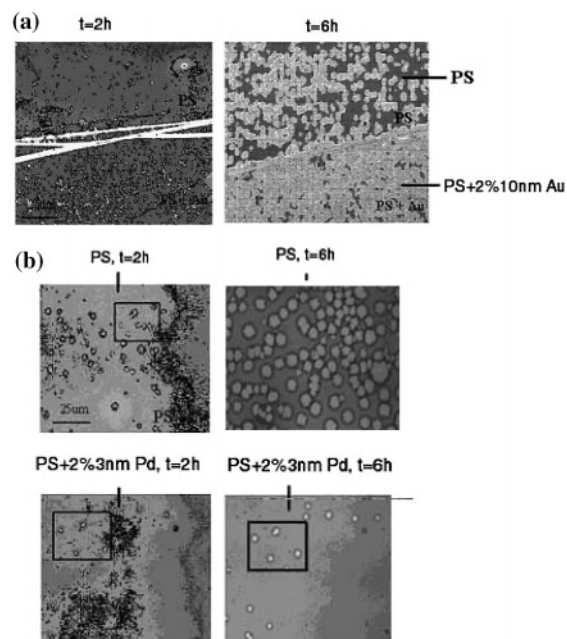

Figure 5. (a) Optical micrograph of a sample where the top and bottom half are the unfilled and filled 10 nm diameter Au particle films, respectively. Two different annealing times (*t*), 4 and 6 h at 162 °C, are shown for the same region of the sample. (b) Optical micrograph of a sample where the top and bottom are the unfilled and filled 3 nm diameter Pd particle films, respectively. Two different annealing times, 4 and 8 h at 168 °C, are shown for the same region of the sample. The box in the image designate the individual holes whose growth was studied.

a thick Si wafer. A second layer consisting of a blend of 40% 217K dPS + 60% 200K PS, and 1% and 2%, 3 nm diameter Pd and 10 nm diameter Au particles, respectively, was spun-cast onto a clean glass slide, floated from distilled water bath onto the first layer. The bilayer samples were annealed under vacuum at 125 °C for up to 10 h. In situ specular neutron reflectivity experiments were performed at the National Institute of Standards and Technology Center for Neutron Research (NCNR), NG-7 reflectometry beamline. The wavelength of neutrons was fixed at $\lambda = 4.7$ Å, and the slit settings were adjusted to fix the resolution at a constant dq/q value ranging from 0.02 to 0.15.

Results and Discussion

Figure 5a is an optical micrograph of a sample with PS of $M_w = 123K$ where the top and bottom half are the unfilled[23] and filled Au particle films, respectively. Two different annealing times, 2 and 6 h (162 °C for the 10 nm diameter Au and 168 °C for the 3 nm diameter Pd particles), are shown on the left- and right-hand side of the image. From this figure one can see that the number of holes is greater on the 10 nm diameter Au-filled half of the sample. Comparing the images from the two annealing times, we find that the dewetting rate of the PS with 10 nm diameter Au nanoparticles is faster. In Figure 5b, we show a similar image where the top and bottom half are the unfilled and filled PS and the 3 nm diameter Pd samples. Here we find that both the number and the rate of growth of the holes are smaller in the 3 nm diameter Pd-filled section of the sample, relative to the unfilled section.

To determine the dewetting velocity, the diameters of approximately 8−10 holes were measured and averaged as a function of annealing time. The box shown in Figure 5a,b shows a representative group of holes whose growth rate was followed as a function of annealing time. The error on the hole diameter measurement was less than 10% and obtained from an average of six holes. Note that the holes selected were well separated
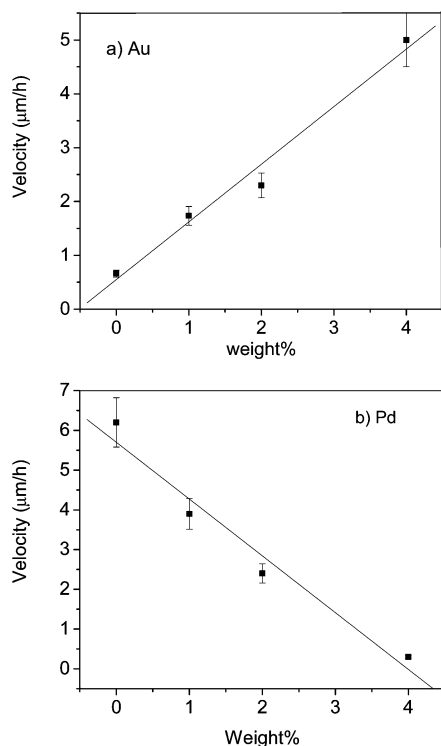
Figure 6. Dewetting velocity vs concentration for $M_w = 123K$ PS films with (a) 10 nm diameter Au particles and (b) 3 nm diameter Pd particles.

Figure 7. TEM micrograph of bilayer samples with 2% of (a) 3 nm diameter Pd and (b) 10 nm diameter Au nanoparticles, annealed for 1 h.

so that the individual growth rates were not affected by the presence of neighboring holes. The dewetting velocities as a function of filler concentrations are plotted for both 10 nm diameter Au and 3 nm diameter Pd-filled films of $M_w = 123K$ in parts a and b of Figure 6, respectively, where we can see that all curves are well fit by linear functions.

From eq 2, we can postulate that this phenomenon is due to a change in the viscosity of the PS films caused by the presence of the nanoparticle fillers. The increase in viscosity with addition of fillers is a well-known phenomenon and has been explained in terms of increasing internal friction due to particle filler interactions by the Einstein relation

$$\mu = \mu_0(1 + 2.5c) \tag{4}$$

Here μ is the viscosity of the filler's liquid, μ_0 is that of the unfilled one, and c is the weight fraction of the filler.

Furthermore, the decrease in effective viscosity observed for the 10 nm diameter Au-containing samples could not be explained at all in the classical model. This model considers the polymer matrix to be a viscous fluid without internal structure. In our case the films are of molecular dimensions, and clearly a more detailed model which considers the configurations of the individual polymer chains relative to the particles is needed to explain these data.

Figure 7 is a TEM micrograph of samples containing 2% 10 nm diameter Au or 3 nm diameter Pd samples that were annealed for 1 h. Comparing with Figure 2, we can see that no significant clustering occurs upon annealing. Furthermore, when the holes are small, particle clusters are not observed at the center of the holes and hence are not responsible for nucleating the holes. In fact, in the 10 nm diameter Au case we observe an increase in particle concentration around the perimeter of the hole. Even though the interaction with the fillers is at best weak, they appear to temporarily pin segments of the film at the edge of the hol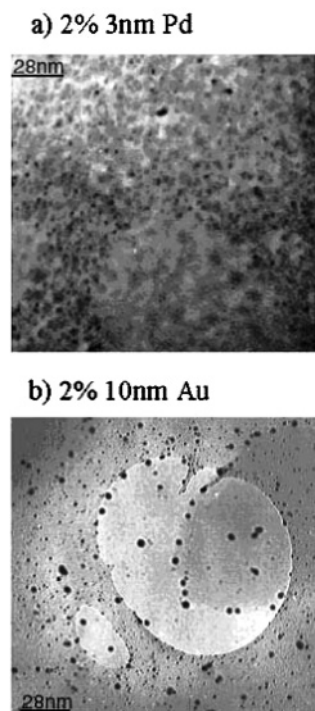es. As the holes expand, the polymer is seen to flow around the particles, which are left behind in the exposed regions. These particles then form large clusters, which appear in the SPM images shown below.

SPM analysis of the holes is shown in Figure 8a,b where we show both topographical and lateral force images. At low concentration (<1%) the holes appear quite spherical in shape with a well-defined rim for both types of particles (not shown). The depth of the holes in both cases is ~32 nm, which is comparable to the film thickness, indicating that dewetting occurs at the interface. The large contrast observed in the lateral force images indicates that the PMMA substrate is exposed inside the holes. From the TEM images of the holes at early stages, we know that the particles clusters are not needed to nucleate the holes and in fact are probably formed from particles that were left behind in the holes' region by the receding PS films.

In Figure 8a,b we show the SPM scans for samples with higher particle concentrations (2% and 4% for Au and Pd, respectively). From the figures we see that in both cases the holes are no longer spherical in shape. This is in contrast to the PS dewetting process where the diameter of the holes increases and the rims grow and maintain their original round shape.[9] An expanded view of several holes (right) shows polymer fibrils, roughly several R_g in diameter, wrapped around the particle clusters (inset of Figure 8a). These fibrils are similar to the ones also seen in the TEM image (Figure 7), at early stages of the hole-opening process. Hence, in order for the PS edge to recede, individual fibrils must first disentangle from the particles, giving the holes a flowerlike appearance. Furthermore, the patterns are highly irregular, since the degree of attachment varies greatly within the hole. This distinguishes this phenomenon from the highly regular and almost fractal appearance observed when dewetting occurs in the presence of evaporating solvents.[24] This phenomenon is even more pronounced in the case of the Pd nanoparticles, shown in Figure 8b. Here we see that nearly all particle clusters are surrounded by polymer. Since the particle diameters are smaller than R_g, the entanglement with the polymers is even stronger.

a) PS+2%10nm Au
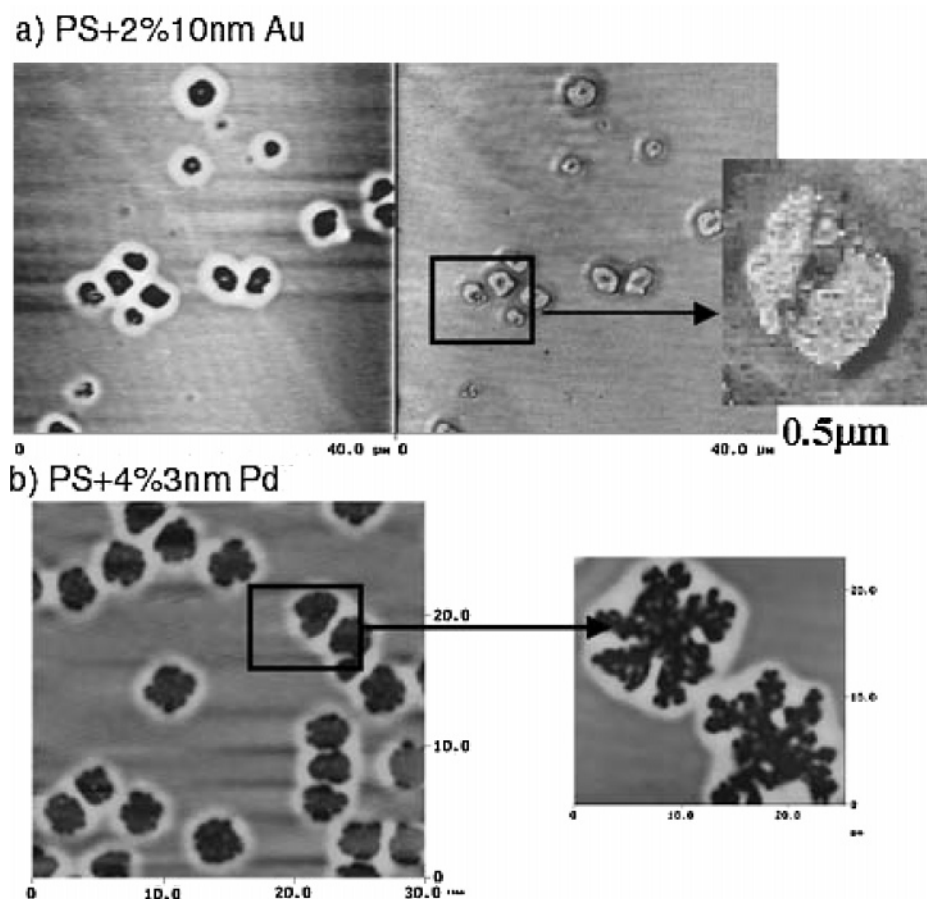
b) PS+4%3nm Pd

Figure 8. (a) Lateral force (left) and topography (right) images of holes in a PS with 2% 10 nm diameter Au particles. The arrow marks an expanded view of the lateral force image. The particles are harder than the substrate and appear dark. PMMA substrate has a larger polymer−tip interaction and appears brighter than the PS. PS fibrils are seen attached to Au clusters in the center, distorting the shape of the holes. (b) Topographical images of a PS film (M_w = 123K) with 4% 3 nm diameter Pd particles. An expanded view shows polymer fibrils attached to the clusters giving them a characteristic flowerlike appearance.

Samples were also observed at later stages where droplets have already formed. In both cases the contact angles, θ, are nearly equal and similar to those previously reported for the unfilled PS/PMMA system.[11] This indicates that the difference in the dewetting is only due to a change in polymer dynamics and hence viscosity. This contrast is due to a change in interfacial energy, which would result if the particles were acting as a surfactant placed which would increase or reduce the interfacial tension between phases.

Figure 9 shows the neutron specular reflectivity (NR) profiles as a function of $q_z = 4\pi \sin(\theta)/\lambda$ for 1% 10 nm diameter Au bilayer samples and annealed at 125 °C. The inset of the figure is the plot of volume fraction of dPS as a function of thickness. From the inset of the figure, we can see that the interfacial width (σ) increases as the annealing time increases. The interfacial width ($\sigma^2/4$) of the samples was plotted as a function of annealing time in Figure 10. The slope of the straight line represents the tracer diffusion coefficient (D). As shown in this figure, the diffusion coefficient, $D = 0.45 \pm 0.01$ Å²/s, for the sample containing 1% of the 10 nm Au particles is significantly higher than the D of the sample containing 1% of the 3 nm diameter Au particles ($D = 0.15 \pm 0.01$ Å²/s). The latter value though is similar to that for the unfilled system, $D = 0.14 \pm 0.01$ Å²/s. The zero shear rate viscosity can then be calculated from the tracer by the Einstein equation

$$D = K_b T/[\eta_0 K_b/G(M)F(M,\nu)] \qquad (5)$$

where K_b is the Boltzmann constant, $F(M,\nu)$ depends on the

microstructure parameters of the polymer, and $G(M)$ is a function related to the entanglement molecular weight obtained from the shear modulus on the rubbery plateau. Using ref 25, we found $G(M) = 10^{-28}$ Nm/K and $F(M,\nu) = 11.5 \times 10^{12}$ m⁻¹. Substituting the D values from the NR experiments into the Einstein equation, we found that within experimental error η_0 is the same for the unfilled system and the 1% 3 nm diameter Au filled system ($\eta_0 = 2.7 \times 10^8$ Ns/m²); however, η_0 is decreased by a factor of ~3 for the 1% 10 nm diameter Au-filled system ($\eta_0 = 1.0 \times 10^8$ Ns/m²). Using eq 2, we found that within experimental error that $V_{particle}/V_{PS} \propto \eta_{ps}/\eta_{particle} = 3.33$ for the 10 nm diameter Au particles and 1.42 for the 3 nm diameter Pd particles. This indicates that the ratio of viscosity for dewetting is in good agreement with the ratio of viscosity extracted from the NR experiments, hence confirming by two independent techniques the effect of nanoparticle size on the effective viscosity of a filled polymer.

To correlate our findings with changes in the glass transition temperature, we used the shear modulation force microscopy method (SMFM) to determine the T_g of the films. The results are shown in Figure 12. Here we plot the modulation amplitude, Δx, vs temperature for a PS film of M_w = 200K, without fillers and with 2% 10 nm diameter Au and 3 nm diameter Pd fillers. As shown previously,[16,17] the discontinuity in the modulation amplitude corresponds to the glass transition temperature where the zero-frequency modulus of the film decreases abruptly. From the figure we can see that, as previously reported,[16,17] the glass transition of the unfilled PS film, T_g = 374 K, is unchanged
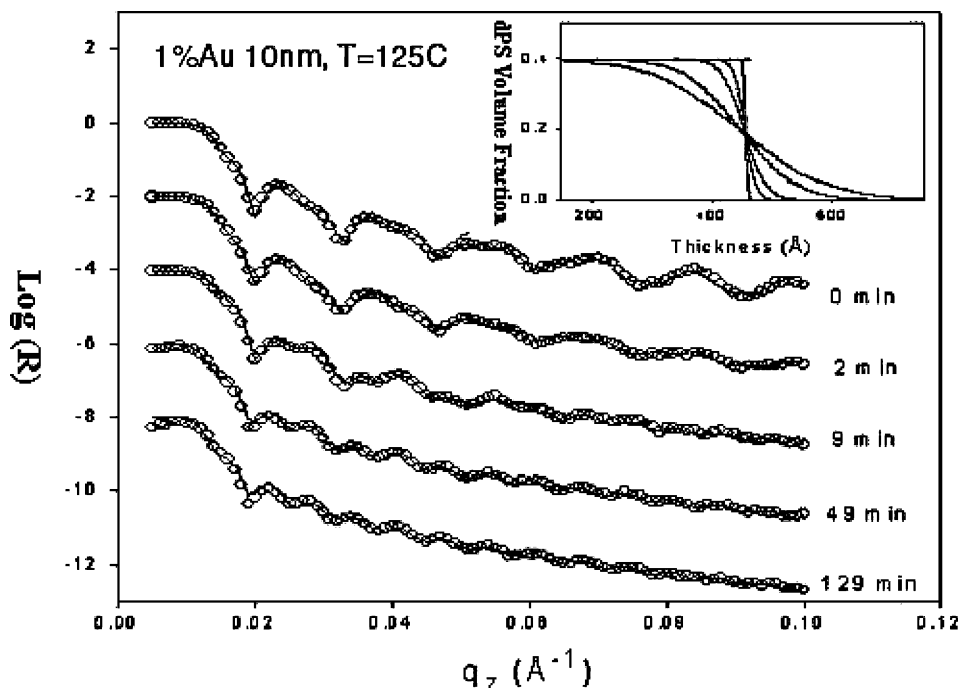
Figure 9. Neutron specular reflecivity profiles as a function of $q_z = 4\pi \sin(\theta)/\lambda$ [(40% 217K dPS + 60% 200K PS + 1% Au 10 nm), ~500 Å)/200K PS, ~500 Å/Si].
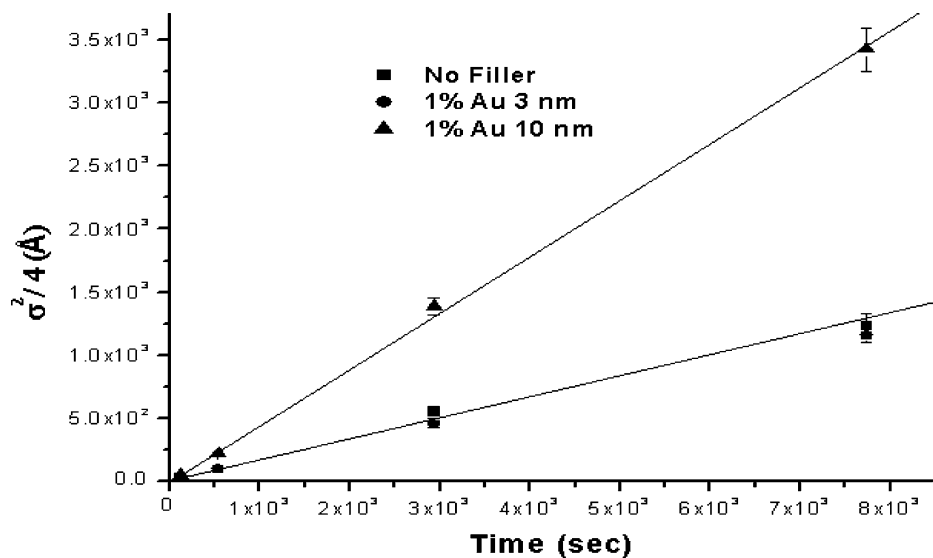

Figure 10. Plot of interfacial width ($\sigma^2/4$) vs time. The slope of each line is diffusion coefficient (*D*). For 1% Au 10 nm, $D = 0.45 \pm 0.01$ Å^2/s. For 1% Au 3 nm, $D = 0.15 \pm 0.01$ Å^2/s. For no fillers, $D = 0.14 \pm 0.01$ Å^2/s.

relative to the bulk value, $T_g = 374$ K. Addition of 2% 10 nm diameter Au particles to the film decreases T_g to 363 °C. These results are in qualitative agreement with the predictions of Glotzer et al.,[26] who used molecular dynamics calculations to simulate a polymer melt surrounding faceted filler, where the facet size was larger than R_g of the chain. They found that when the interaction between the polymer and the facets was weaker than the interaction between the monomers in the melt, as is the case in this study, T_g of the melt was reduced due to an increase in the excluded volume. This group has not yet considered the case when the facet size is smaller than R_g. On the other hand, it is reasonable to assume that when the filler size is on the order of several polymer segments, i.e., less than R_g, full adsorption of the chains is not possible, and hence increase in free volume would not occur. This may be a possible explanation for the fact in the film with 2% 3 nm diameter Pd

particles $T_g = 371$ K is virtually unchanged relative to the bulk value.

Until now, we varied the size of the filler while keeping the interactions and the matrix molecular weight constant. We can also probe out hypothesis by varying the molecular weight of the polymer while keeping the particle size fixed. The data of Δx vs temperature for a film of $M_w = 4M$ g/mol with 2% 10 nm diameter Au filler is plotted as open diamonds in Figure 11. In this case the ratio of the polymer radius, R_g, relative to the radius of the Au particles, $R = 8.9$, is comparable to $R = 8$ obtained for the Pd particles in the $M_w = 200K$ PS matrix. From Figure 11 we can clearly see that T_g has now increased to 372 K or close to the bulk value.

The increase in T_g is also reflected in the dynamics of the high-molecular-weight PS films filled with the 10 nm diameter Au particles. In Figure 12 we plot the diameter of dewetting
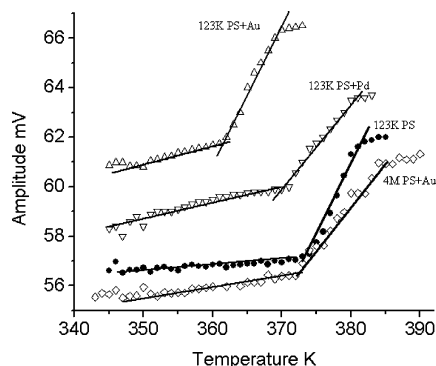
Figure 11. Modulation amplitude, Δx, vs temperature for unfilled bilayer samples with PS ($M_w = 200K$) and bilayers containing 2% 3 nm diameter Pd and 10 nm diameter Au particles together with a sample of $M_w = 4M$ g/mol and 2% 10 nm diameter Au particles.
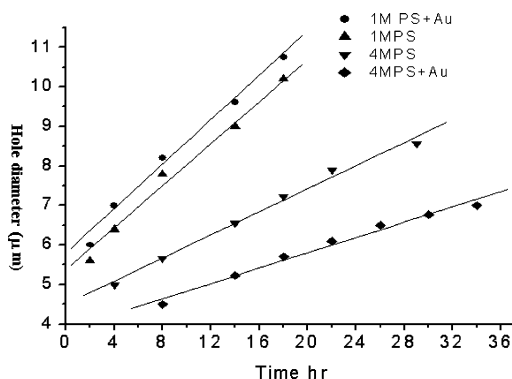
Figure 12. Hole diameter vs annealing time for filled (2% 10 nm diameter Au particles) and unfilled films, $M_w = 1M$ and 4M g/mol.
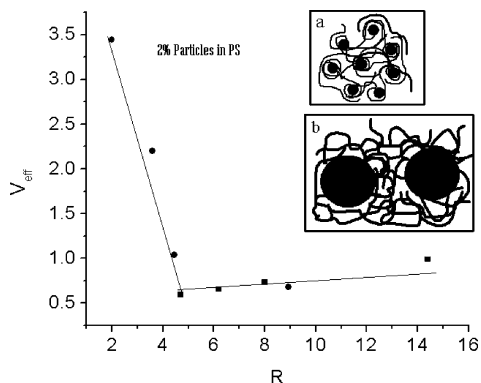
Figure 13. $V_{eff} = V_{particle}/V_{PS}$ plotted vs $R = R_g/R_{particles}$ for both 10 nm diameter Au and 3 nm diameter Pd particles at 2% in PS matrices of different molecular weights. The inset is a sketch of filled particle−polymer system. (a) When $R > 1$ and (b) when $R \ll 1$.

holes formed on the PMMA, from which we can extract the velocities of unfilled and filled (2% 10 nm diameter Au) PS films of $M_w = 1M$ g/mol and 4M g/mol.[28] We can see that the lines are nearly parallel for the $M_w = 1M$ g/mol the filled and unfilled PS film, while for PS of $M_w = 4M$ g/mol the slope is significantly lower for the filled system. From this we can conclude that the dewetting velocity of the filled system is significantly slower than the unfilled control. In Figure 13 we plotted the ratio between the dewetting velocities of the filled (2% fillers) and corresponding unfilled sections of the same sample, $V_{eff} = V_{particle}/V_{PS}$ vs $R = R_g/R_{particles}$, for both the 2% 10 nm diameter Au-filled and 2% 3 nm diameter Pd films. From the graph we see that for a filler concentration of 2% the points condense on a universal curve where the crossover between accelerated and suppressed dewetting velocities, or $V \sim 1$, occurs

when the particle size is roughly $^1/_4$ the size of the polymer chain. The degree of suppression at this filler concentration is roughly a factor of 2 and independent of R, while the acceleration increases linearly with decreasing R.

These results are intriguing, and we hope more work, both experimental and theoretical, needs to be done in order to yield a quantitative model. At this point we can only suggest the qualitative interpretation based on the results obtained so far. The filled particle/polymer systems are sketched as insert in Figure 13 for the case when $R > 1$ and $R \ll 1$. When $R > 1$, the insertion of the particle in the melt causes local deformations of the polymer matrix. Hence, if local relaxation is the driving force, then both the weak dependence on the matrix molecular weight shown in Figure 12 and the increase of V with R can be explained. When the particles are roughly the size of a polymer segment, chain deformation does not occur, and no excess free volume is introduced. Consequently, decreasing the dimensions of the particles further should have only a minimal effect on the local dynamics, which are consistent with reptation. Since the driving force for dewetting is analogous to applying a local shear in the film, it may be that the smaller particles are in fact reinforcing the polymer against rupture, but more work needs to be done in order to establish this phenomenon.

Conclusion

In conclusion, we have carried out a systematic study of the effect of fillers on the dewetting dynamics of PS films on a PMMA substrate. From X-ray reflectivity and TEM microscopy we observed that no segregation of the particles occurred to any of the interfaces, and clustering was minimal during the observation times. The results show that the dynamics are a sensitive function of the ratio between the filler and the host polymer radius of gyration. The data all collapse on a universal curve where we find that the relative velocity of the filled system was faster than that for the unfilled system when $R_g/R_{particle} > 4$ and slower when $R_g/R_{particle} < 4$. To confirm these findings, the viscosity ratio was also measured using neutron reflectivity. Here we applied the Einstein relation to deduce the viscosity from measurements of the tracer diffusion coefficient. The results indicated that the viscosity decreased by a factor of 3.3 with the addition of 1% 10 nm diameter particles, while remaining nearly unchanged with the addition of 1% 3 nm diameter particles. These results are in good agreement with the viscosity deduced from dewetting measurements.

The change in viscosity was further probed by SMFM measurements as a function of temperature. The results indicated that T_g was depressed by 12 °C relative to the bulk value above the cutoff and bulk like below the cutoff. These results were interpreted in terms of an increase in the excluded volume when large particles were introduced into the matrix. When the particle diameters were smaller than $R_g/4$, they were able to fit within the chain segments and did not cause any change in the overall entropy or free volume of the system. In this paper we confine ourselves to the case of weakly interacting fillers where we focused only on the relative dimensions between the filler and matrix chains. Work is currently in progress where we keep the relative dimensions constant while varying the interactions.

References and Notes

(1) Lisari, J. J. *Plastic Coatings for Electronics*; McGraw-Hill: New York, 1970.

(2) Cowie, J. M. G. *Polymers: Chemistry and Physics of Modern Materials;* Chapman and Hall: New York, 1991.

(3) Singh, J.; Agrawal, K. *Chem. Phys.* **1992**, *32*, 521.

(4) Bhattacharya, S. K. *Metal-Filled Polymers: Properties and Applications;* Dekker: New York, 1986; p 17.

(5) Barnes, K. A.; Karim, A.; Douglas, J. F.; Nakatani, A. I.; Grull, H.; Amis, E. J. *Macromolecules* **2000**, *33*, 4177.

(6) Luo, H.; Gersappe, D. *Macromolecules* **2004**, *37*, 5792.

(7) Sharma, S.; Rafailovich, M. H.; Peiffer, D.; Sokolov, J. *Nano Lett.* **2001**, *10*, 511.

(8) Balazs, A. C.; Ginzburg, V. V.; Qiu, F.; Peng, G.; Jasnow, D. *J. Phys. Chem. B* **2000**, *104*, 3411.

(9) Cole, D. H.; Shull, K. R.; Baldo, P.; L. Rehn, L. *Macromolecules* **1999**, *32*, 771. Mackay, M. E.; Dao, T. T.; Tuteja, A.; Ho, D. L.; Horn, B. V.; Kim, H. C.; Hawker, C. J. *Nat. Mater.* **2003**, *2*, 762.

(10) Qu, S.; Clark, C. J.; Liu, Y.; Sokolov, J.; Rafailovich, M. H. *Macromolecules* **1997**, *30*, 3640.

(11) Brochard-Wyart, F.; Martin, P.; Redon, C. *Langmuir* **1993**, *9*, 3682. Brochard-Wyart, F.; Daillant, J. *Can. J. Phys.* **1990**, *68*, 1084.

(12) Yee, C. K.; Ulman, A.; Sokolov, J.; Rafailovich, M. H. *Langmuir* **1999**, *15*, 3486.

(13) Seeman, R.; Herminghaus, S.; Jacobs, K. *Phys. Rev. Lett.* **2001**, *87*, 196101.

(14) Sferrazza, M.; Xiao, C.; Jones, R. A.; Bucknall, D. G.; Webster, J.; Penfold, J. *Phys. Rev. Lett.* **1997**, *78*, 3693.

(15) Jaeger, R. C. *Intro to Microelectronics Fabrication;* Addison-Wesley: Reading, MA, 1993; Vol. 5.

(16) Kern, W.; Puotinen, D. A. *RCA Rev.* **1970**, *31*, 187.

(17) Pu, Y.; Ge, S. R.; Rafailovich, M.; Sokolov, J.; Duan, Y.; Pearce, E.; Zaitsev, V.; Schwarz, S. *Langmuir* **2001**, *17*, 19, 5865.

(18) Ge, S.; Pu, Y.; Zhang, W.; Rafailovich, M.; Sokolov, J. *Phys. Rev. Lett.* **2001**, *85*, 11.

(19) Slep, D.; Asselta, J.; Rafailovich, M.; Sokolov, J.; Winesett, A.; Smith, A. P.; Ade, H.; Anders, S. *Langmuir* **2000**, *16*, 5, 2369.

(20) Helfand, E.; Tagami, Y. *Polym. Lett.* **1971**, *9*, 741.

(21) Young, T. *Philos. Trans. R. Soc. London* **1805**, *5*, 65.

(22) Ulman, A. *An Introduction to Ultrathin Organic Films: From Langmuir-Blodget to Self-Assembly*; Academic Press: New York, 2001.

(23) Sharma, S.; Rafailovich, M. H.; Sokolov, J.; Liu, Y.; Qu, S.; Schwarz, S. A.; Eisenberg, A. *High Perform Polym* **2000**, *12*, 581.

(24) Lee, S. H.; Yoo, P. J.; Kwon, S. J.; Lee, H. H. *J. Chem. Phys.* **2004**, *121*, 4346.

(25) Green, P. F.; Kramer, E. J. *Macromolecules* **1986**, *19*, 1108.

(26) Starr, F. W.; Schroder, T. B.; Glotzer, S. C. *Phys. Rev. Lett. E* **2001**, 64. Chatterjee, A. P.; Schweizer, K. S. *J. Chem. Phys.* **1998**, *109*, 10477.

(27) It should be noted that the intercept of the curves is not at zero. The holes initially open due to nucleation around defects or strains in the film as a mechanism for strain release. Consequently, at very early times the opening velocities are not driven by viscous forces and do not follow the relationship given by eq 2 from ref 11.

(28) Plazek, D. J.; O'Rourke, V. M. *J. Polym. Sci., Part A-2* **1971**, *9*, 209.